Macromolecular Rapid Communications
www.mrc-journal.de

Aqueous Dispersions of Polypropylene: Toward Reference Materials for Characterizing Nanoplastics

*Jana Hildebrandt and Andreas F. Thünemann**

Microplastics and nanoplastics pollute the natural environment all over the world, but the full extent of the hazards posed by this waste is unclear. While research on microplastics is well advanced, little work has been done on nanoplastics. This discrepancy is mainly due to the lacking ability to detect nanoplastics in biologically and environmentally relevant matrices. Nanoplastics reference materials can help the development of suitable methods for identifying and quantifying nanoplastics in nature. The aim is to synthesize nanoplastics made from one of the most commonly used plastics, namely polypropylene. An easy way to produce long-term stable aqueous dispersions of polypropylene nanoparticles (nano polypropylene) is reported. The nanoplastic particles, prepared by mechanical breakdown, show a mean hydrodynamic diameter of $D_h = 180.5 \pm 5.8$ nm and a polydispersity index of PDI $= 0.084 \pm 0.02$. No surfactant is needed to obtain dispersion which is stable for more than 6 months. The colloidal stability of the surfactant-free nano polypropylene dispersions is explained by their low zeta potential of $\zeta = -43 \pm 2$ mV.

1. Introduction

Plastic nanoparticles—a.k.a. nanoplastics—are assumed to be becoming increasingly abundant in nature.[1] This is because global plastic production is increasing and waste is not being disposed of properly in large parts of the world. No strategies are in place for reusing or recycling plastics produced as completely as possible, which would otherwise prevent them from entering the environment. Only about 21% of plastic produced between 1950 and 2015 has been reused through recycling or incineration, leaving 79% that has ended up in landfills or otherwise entered the natural environment.[2] There, various degradation processes turn macroplastics into microplastics and ultimately nanoplastics. An awareness of these processes and the possible negative effects of microplastics is evident in large sections of the population nowadays.

For clarity, it should be noted that in addition to the international standard ISO/TR21960:2020(en), Hartmann et al. have suggested that nanoplastic particles refer to dimensions < 1μ m.[3] We refer to both publications for definitions and classifications for plastic debris. In contrast, Sieg et al.[4] have decided to use the term "nano" as commonly used in the nanotoxicology field,[5] whereby nanoplastic refers to particles ranging from 1 to 100 nm. In the literature, there is often a gap in the definition between the lower size limit for microplastics (>1 μm) and the size range for nanoparticles below 100 nm. For the plastic particles with diameters between 100 and 1000 nm the term "submicron" is often used.[4]

Recently, Paul-Pont et al.[6] recommended that laboratory studies on microplastics made of the "Big Six" polymers, that is, polypropylene (PP), polyethylene (PE), polyvinyl chloride (PVC), polyurethane (PU), polyethylene terephthalate (PET), and polystyrene (PS), so that priorities could be set for experimentally exposing of marine organisms to these plastics. These polymers account for 80% of the plastics produced in Europe. Polypropylene and polyethylene can be focused on even more because recoveries of these two polymers dominate in all environmental compartments. For example, polyethylene accounts for 53–67% and polypropylene for 16–30% of the plastics found in the Bay of Brest.[7] Due to the lack of comparable data for nanoplastics, we assume that the occurrence of polyethylene and polypropylene as nanoplastics is comparably high.

In contrast to microplastic, data available on nanoplastics is scarce.[8] This also means that the risk assessment for nanoplastics is still in its infancy. Some studies, however, give considerable cause for concern. As one example, Tallec et al. found that nanoplastics induced a significant decrease in fertilization success as well as embryo–larval development amongst Pacific oysters, while no effects of plain microplastics were seen.[9] Hollóczki and Gehrke reported that polyethylene nanoparticles dissolve in the hydrophobic core of lipid bilayers in a simulation study.[10] Accordingly, there is also a risk that vital functions of the cell membranes might be altered. The same authors reported that nanoplastics can change the secondary structure of proteins.[11] In this case, the danger is that such proteins might lose their function, whereby enzymes might become inactive as one example.

J. Hildebrandt, A. F. Thünemann
Bundesanstalt für Materialforschung und -prüfung (BAM)
Unter den Eichen 87, 12205 Berlin, Germany
E-mail: andreas.thuenemann@bam.de

The ORCID identification number(s) for the author(s) of this article can be found under https://doi.org/10.1002/marc.202200874

DOI: 10.1002/marc.202200874

In general, there are two ways that previous studies of nanoplastic toxicity have proceeded. One part of the studies uses spherical plastic nanoparticles, mostly made of polystyrene (PS), whose size is known.[12] These nanospheres are available for purchase and therefore easily accessible to the user. At the same time, these commercial nanospheres were not produced for the purpose of serving as reference materials for nanoplastics found in the environment. Added additives and surfactants can falsify results.[13] Therefore, more and more research groups are moving toward producing their own test material.[14] However, the quantities produced are often only sufficient for one study and do not allow comparison between different laboratories. An easily repeatable method with stable results concerning the size of the particles is therefore much needed. In this study, we produced long-term stable aqueous dispersions of polypropylene nanoparticles from bulk material. The presented preparation method for polypropylene nanoparticles was inspired by the approach proposed by Ekvall who formed nanoplastics by mechanically breaking of polystyrene products used in daily life.[15] The authors produced polystyrene nanoplastics directly in water using a household immersion blender. Ekvall et al. also recently reported on nanoplastics of high-density polyethylene displaying a diameter around 110 nm which induced a size-dependent toxic effect in the zooplankton species *Daphnia magna*.[16] In their method, the prepared polyethylene particles were not stable in solution over time, that is, no nanoparticles were detected after a storage time of 100 days. Very likely, their ζ potential of about -10.9 ± 6.4 mV was not sufficient to allow for colloidal long-term stability. Highly stable particles could be expected for ζ potentials below -30 mV.[17] Since we wanted to avoid using surfactant stabilizers, establishment of a strongly negative zeta potential was the most important goal for providing colloidally stable dispersions. In the following, we show how this was possible for polypropylene nanoparticles. In the future, these dispersions are intended to serve as reference materials for the detection of nanoplastics in liquid samples. Such reference materials might help in the development of methods for detecting polypropylene nanoplastics in food and environmental samples.

2. Results and Discussion

Mechanical breakdown was used to crush macroscopic polypropylene granules into smaller pieces by employing a mechanical disperser based on the rotor–stator principle, thereby providing a higher mechanical energy input than that utilized by Ekvall.[15] Preparing polypropylene nanoparticles directly in water proved unsuccessful, but success was achieved when using acetone as the dispersion medium while crushing the polypropylene granules at a temperature of 0 °C. Larger polymer fragments were removed after mechanical breakdown via filtration, then water was added, and the acetone was finally removed by distillation. In this form it remains as an aqueous phase, displaying the typical semitransparent appearance of a diluted particle dispersion, as can be seen in **Figure 1**. We assume that polypropylene is brittle enough under the chosen conditions to form a significant number of separated nanoparticles, which at the same time are colloidally stabilized. We also assume that processes such as polymer welding, which counteract the formation of colloids, predominate in pure water.

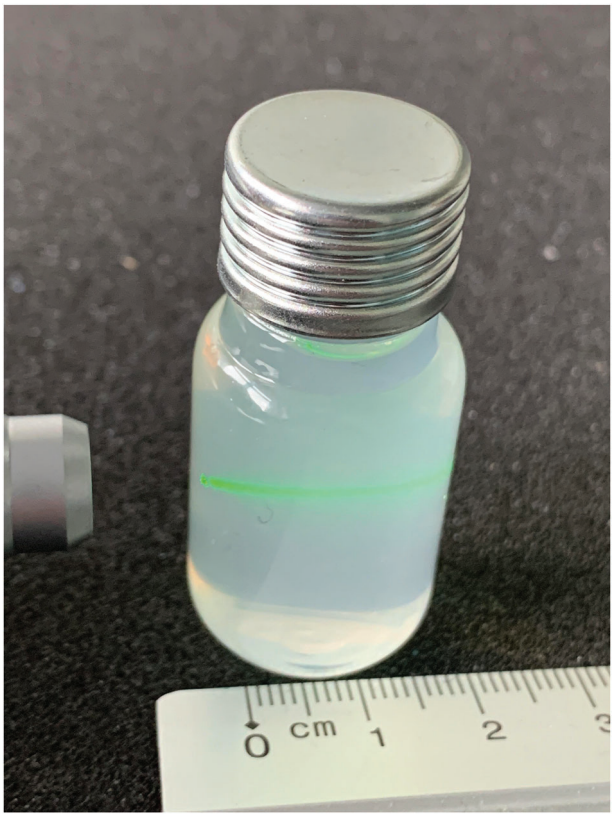

Figure 1. Bottle containing 10 mL of an aqueous dispersion of polypropylene nanoparticles. The dispersion is illuminated with a green laser from the left side to illustrate the light scattering properties.

As such, polypropylene nanoparticles are not formed in water without the help of surfactants. Recently, Lionetto et al. reported on the production of PET nanoparticles via a stepwise grinding and sieving of PET pellets.[18] Like our observations, their work also suggests that high mechanical energy input typically causes nanoparticles to re-weld if they are not immediately colloidally stabilized. Polystyrene on the other hand is brittle at ambient conditions, which may explain the fact that re-welding processes failed to prevent the formation of PS nanoparticles in the study of Ekvall.[15] It seems plausible to us that the formation of nanoparticles by grinding becomes more difficult as the glass transition temperature of the polymer increases. The glass transition depends not only on the material, but also on the pretreatment of the polymer. Nevertheless, the glass transition temperature and thereby the ease of preventing re-welding increases in the order PE (−100 °C), PP (−10 °C), PET (70 °C) to PS (100 °C).

Since our polypropylene nanoparticles are dispersed in pure water without any added stabilizer, we assumed that the particles start to agglomerate after short periods of storage. To test this assumption, a sample was filled into a glass vial and left at ambient room temperature and under lighting. The hydrodynamic diameter of the particles of this sample was then measured at 0, 9, 43, and 245 days after sample preparation. Surprisingly, no signs of agglomeration could be found in the DLS data and the hydrodynamic diameter stayed constant at 116 ± 10 nm as can

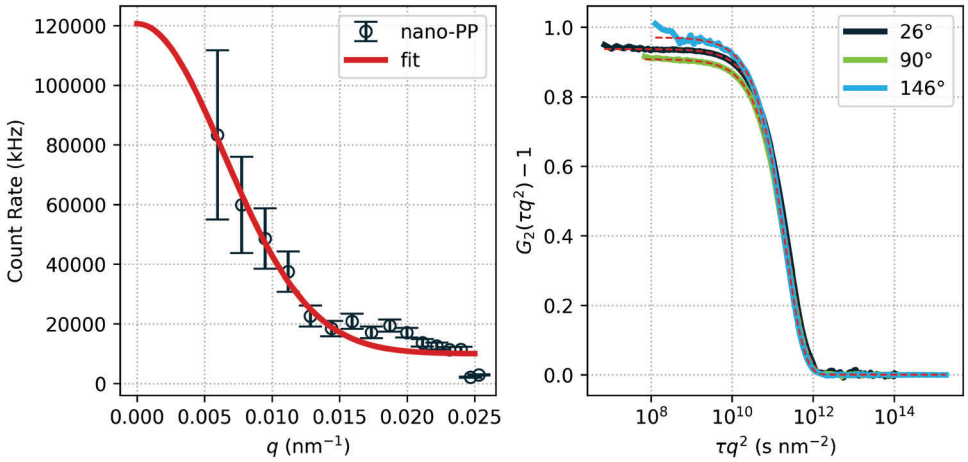

Figure 2. Light scattering. Left panel: SLS data (circles) and Guinier approximation according to Equation (1) (red solid line) providing a radius of gyration of R_g = 190.8 ± 6.9 nm. Right: Intensity correlation functions of measurements performed at scattering angles of $2\theta = 26°$, 90°, and 146°, respectively. The red dotted lines represent curve fits using Equation (4).

Table 1. Molecular characteristics of the polypropylene before and after nanoparticle preparation, as derived by gel permeation chromatography. $\bar{M}_n$ is the number-weighted mean molar mass, $\bar{M}_w$ is the mass-weighted mean molar mass, and Đ is the dispersity index.

	$\bar{M}_n$ (g mol^{-1})	$\bar{M}_w$ (g mol^{-1})	Đ
Pristine polypropylene	1.1· 10^4	3.6· 10^4	3.3
Nano polypropylene	1.2· 10^4	3.6· 10^4	2.9

be seen in Figure S2, Supporting Information. This finding indicates that no additional stabilizing surfactants are necessary to create a long-term stable aqueous dispersion of the polypropylene nanoparticles. Therefore, the assumption that this method might be suitable for producing a reference material seemed justified. To increase the concentration of the nanoparticles, a higher concentration of granular starting material was then used to produce the nanoparticle reference material candidate, resulting in a polypropylene weight concentration of 41 µg mL^{-1} as determined gravimetrically (see Experimental Section).

The particle preparation was suspended in acetone because acetone forms no azeotrope with water,[19] and is easily removable from an acetone/water mixture by evaporation due to its low boiling temperature of 56 °C. There was a possibility that the polypropylene chains might have been mechanochemically cleaved and that the acetone may have reacted with the subsequently produced polymer fragments. For this reason, gel permeation chromatography was performed on the pristine polypropylene and on dried nano polypropylene to test this hypothesis. This showed that the number-weighted mean molar mass $\bar{M}_n$ of (1.1 − 1.2) × 10^4 g mol^{-1}, the mass-weighted mean molar mass $\bar{M}_w$ of 3.6 × 10^4 g mol^{-1} and the dispersity index Đ of 2.9 to 3.3 did not change significantly due to particle preparation, that is, the main characteristics of the molecular weight distribution were unchanged (see also **Table 1**). This result strongly indicates that the polypropylene chains themselves remain unchanged in the process of preparing nano polypropylene.

2.1. Size Determination

The sizes of the produced polypropylene particles were determined by static (SLS) and dynamic light scattering (DLS). The intensity values of the SLS data as a function of the scattering vector $I(q)$ are bell shaped, indicating the presence of defined particles. The SLS data were interpreted using the Guinier approximation[20]

$$I(q) = I_0\, e^{-R_g^2 q^2/3} \tag{1}$$

where I_0 is the scattering intensity at a scattering vector of q = 0 and R_g is the particles' radius of gyration. The relationship between the radius of a sphere and its radius of gyration is $R^2 = 5/3R_g^2$. Together with $R = D/2$, one obtains $D = 2\sqrt{5/3}R_g$, where D is the equivalent sphere diameter. The radius of gyration was R_g = (190.8 ± 6.9) nm, corresponding to an apparent diameter of D = (490 ± 18) nm. SLS data and curve fits according to Equation (1) are shown in **Figure 2**.

Multi-angle DLS was used to characterize the hydrodynamic diameter of the particles, as well as to indicate aggregation and particle–particle interaction. The intensity correlation functions of the DLS measurements were approximated by Friskens' variation of the cumulants' method.[21] This method utilizes direct curve fittings of the measured intensity correlation functions with

$$G_2(\tau) - 1 = B + \beta \exp\left(-2\bar{\Gamma}\tau\right)\left(1 + \frac{\mu_2}{2!}\tau^2\right)^2 \tag{2}$$

where B is a baseline, $\bar{\Gamma}$ is the first cumulant (mean decay rate), and μ_2 is the second cumulant. The third and higher cumulants are normally considered as not significant[21] as already stated by Koppel.[22] The $\bar{\Gamma}$ is related to the mean translational diffusion coefficient $\bar{D}$ of the particles by $\bar{\Gamma} = \bar{D}q^2$, where $q = 4\pi n/\lambda \sin(\theta)$ is the scattering vector. The n =1.332 is the refractive index of water, λ = 632.8 nm the wavelength of the laser, and 2θ is the

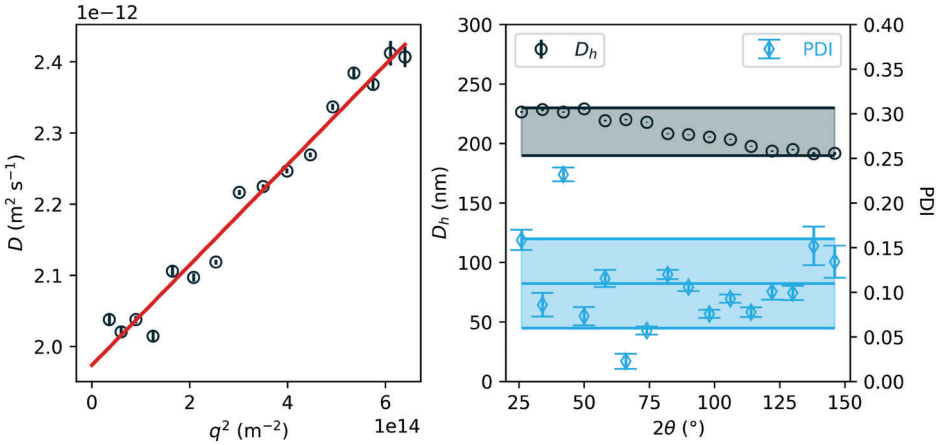

Figure 3. Light scattering. Left panel: Diffusion coefficients as a function of q^2 (circles) and a linear fit (red solid line). Right panel: Hydrodynamic diameter (black circles) and PDI (blue diamonds) at different scattering angles. The gray area covers the range between the smallest and largest D_h-value of 190 and 230 nm. The blue area comprises the mean value of the PDI plus-minus one standard derivation,that is, <PDI > =0.11 ± 0.05.

respective scattering angle. The diffusion coefficient can be determined directly as a fit parameter when using

$$G_2(\tau) - 1 = B + \beta \exp\left(-2\bar{D}\tau q^2\right)\left(1 + \frac{\mu_2}{2}\tau^2\right)^2 \quad (3)$$

In the graphical representation it is not ideal that the data do not overlap for measurements at different q-values when the diffusion coefficient is the same. For displaying the correlation functions more optimally, an x-axis transformation from τ to $x = \tau q^2$ was therefore performed, as

$$G_2(x) - 1 = B + \beta \exp\left(-2\bar{D}x\right)\left[1 + \frac{\mu_2}{2q^4}x^2\right]^2 \quad (4)$$

This presentation allows direct evaluation from the data whether the $\bar{D}$ and hence the D_h-values are angular dependent. Examples of using Equation (4) for interpretation of the $G_2(\tau q^2) - 1$ data for scattering angles of 26°, 90°, and 146° are given in Figure 2. It is easy to see that the curves are largely superimposed, indicating the absence of aggregates. Nevertheless, a certain systematic angular dependence of the diffusion coefficient is visible, ranging from $\bar{D} = 2.0 \times 10^{-12}$ to 2.4×10^{-12} m^{2}s^{-1}, as shown in **Figure 3**. The $\bar{D}$ values increase approximately linearly with q^2 as

$$\bar{D} = (1.97 \pm 0.02) \times 10^{-12}\mathrm{m^2s^{-1}} + (7.0 \pm 0.3) \times 10^{-28}\mathrm{m^4s^{-1}} \times q^2 \quad (5)$$

(see the red solid line in the left panel of Figure 3). The $\bar{D}$ and D_h are related by

$$D_h = \frac{kT}{3\pi\eta\bar{D}} \quad (6)$$

with an uncertainty of

$$u_{D_h} = \frac{kT}{3\pi\eta\bar{D}^2}u_{\bar{D}}, \quad (7)$$

where k is the Boltzmann constant, T is the temperature, η is the viscosity of water, and $u_{\bar{D}}$ is the uncertainty of $\bar{D}$ as estimated from the curve fit. Application of Equations (6) and (7) provides a hydrodynamic diameter of $D_h = (230.0 \pm 1.5)$ nm for $\lim_{q^2\to 0}\bar{D}(q^2)$. This D_h value can be assumed to be the most physically realistic value, as this form of evaluation of multi-angle light scattering data has been generally accepted.[23] For application as reference material, however, it is of great importance to consider the measurement capabilities of the typical users and, not just those of national metrological institutes and other excellently equipped facilities. Typically, users have DLS instruments that measure at only one scattering angle, for example, 90° or most often in back scattering mode, that is, at 173°. It is therefore important to specify which hydrodynamic diameter is to be determined for the nano polypropylene for the respective measuring angle of the user's respective measuring instrument. A conversion of the angle-dependent diffusion coefficients, from Figure 2 to hydrodynamic diameters, can be seen in Figure 3. Therein, the minimum value is $D_h = 190$ nm and the maximum value is 230 nm. In principle, it is possible to certify the parameters of Equation (5) for using nano polypropylene as reference material. This allows the reference value to be calculated for the measuring angle of the respective instrument. However, this might be impractical for many potential users. Due to the large number of DLS instruments that operate with a back scattering geometry, it seems appropriate to us to specify a D_h value for a measurement in back scattering mode as a reference value.

A second relevant parameter is the polydispersity index, abbreviated as PI or PDI, and defined as the ratio of the second cumulant and the square of the first cumulant in Equation (A.13) of the ISO 22412 standard.[24] The

$$\mathrm{PDI} = \frac{\mu_2}{\bar{\Gamma}^2}, \text{ and with } \bar{\Gamma} = \bar{D}q^2 \text{ is equivalent to } \mathrm{PDI} = \frac{\mu_2}{q^4\bar{D}^2} \quad (8)$$

The uncertainty of the PDI as calculated according to GUM[25] is

$$u_{\mathrm{PDI}} = \left[\left(\frac{1}{q^4\bar{D}^2}\right)^2 u_{\mu_2}^2 + \left(\frac{2\mu_2}{q^4\bar{D}^3}\right)^2 u_{\bar{D}}^2\right]^{1/2} \quad (9)$$

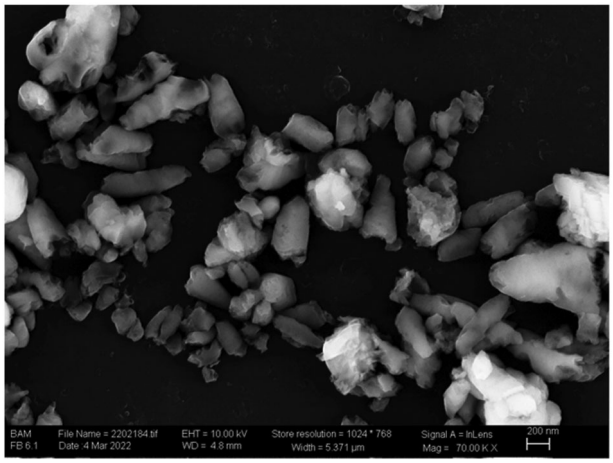

Figure 4. Scanning electron micrograph of polypropylene particles (scale bar = 200 nm).

We found that, in contrast to D_h, the PDI values do not show any systematic dependence on q as can be seen in the left panel of Figure 3 (blue diamonds). The mean value is <PDI > =0.11 ± 0.05 (horizontal blue line) and may serve as a potential reference value. The <PDI > is surprisingly low, considering the production of nano polypropylene via mechanical breakdown.

By comparing the radius of gyration and the hydrodynamic radius according to $\rho = R_g/R_h$, the ρ ratio is obtained,[26] which provides information about the shape of particles. A homogeneous sphere has the smallest possible value for the ρ ratio of 0.775. The ρ ratio increases as the shape changes from spherical to extended rigid particles.[23,27] The ρ ratio of nano polypropylene is in the range of about 1.7 and 2.0 indicating that the nano polypropylene deviates significantly from a spherical shape.

Scanning electron micrograph (SEM) measurements of the polypropylene particles were performed to reveal insights about particle shapes. A typical SEM image is given in **Figure 4**. It is obvious that the particle have clear fracture edges. Additionally, the particle shape appears to be elongated. If we assume a simplified cylinder geometry, we can calculate a hydrodynamic equivalent diameter. For this, we set the diffusion coefficient of a sphere to $D_s = k_B T/(3\pi\eta D_h)$, equal to that of a cylinder of[28,29]

$$D_c = \frac{k_B T}{3\pi\eta l}(\log(p) + \nu) \tag{10}$$

with $p = l/d$ and $\nu = 0.312 + 0.565\,p^{-1} - 0.1\,p^{-2}$, resulting in

$$D_h = \frac{l}{0.313 - 0.1d^2/l^2 + 0.565\,d/l + \log(l/d)} \tag{11}$$

The Boltzmann constant k_B, temperature T, and viscosity η are shortened, that is, D_h is given by length l and diameter d of the cylinder. Inserting a cylinder length of $l = 300$ nm and a diameter of $d = 100$ nm provides a hydrodynamic equivalent diameter of $D_h = 189$ nm. This value is consistent with the experimentally observed hydrodynamic diameters and suggests that the SEM picture is representative of the nano polypropylene. It should be noted here that a detailed SEM/TEM study is underway and is beyond the scope of the current work.

2.2. Zeta Potential

The obvious assumption to explain particle colloidal stability is that the particles are stabilized by surface charges. ζ potential measurements were taken to substantiate this assumption. Indeed, the as-prepared particles revealed ζ potential values of around - 35 mV at pH 7.4. As a general rule (even if the individual case can be more complicated), nanoparticle dispersions with ζ potentials of ± 0–10 mV are classified as highly unstable, ± 10–20 mV as relatively stable, ± 20–30 mV as moderately stable, and larger than ± 30 mV as highly stable.[30–32] We therefore conclude that the strongly negative ζ potential of the nano polypropylene is the cause for its colloidal long-term stability. Next, we measured the ζ potential as a function of the pH by titration with hydrochloric acid. The ζ(pH) data display a sigmoidal shape as shown in **Figure 5**. For quantification, we follow the approach of Creux et al.[31] and fitted the data as an acid–base titration curve with

$$\zeta(\mathrm{pH}) = \frac{\zeta_s K}{10^{-n\,\mathrm{pH}+K}} \tag{12}$$

where ζ_s is the saturation level of the ζ potential at high pH, K is the acid–base equilibrium constant and n is an exponent. Application of Equation (12) provided $\zeta_s = 35\pm1$ mV and $K = (1.13\pm0.12) \cdot 10^{-4}$ (see red solid line in Figure 5). A fixed value of n=1 was employed to avoid ambiguous results. Extrapolation to low pH values provides $\lim_{\mathrm{pH}\to 0}\zeta(\mathrm{pH}) = 0$ mV. The half titration point of $\zeta_s/2 = -17.48$ mV is found at pH 3.94 as indicated by the blue lines in Figure 5.

At first glance, the presence of a strongly negative ζ potential of the nano polypropylene without use of an anionic colloidal stabilizer such as sodium dodecyl sulfate[33] or poly(acrylic acid)[34] seems surprising. Therefore, we must assume that the negative ζ potential is generated by the water itself interacting with the polypropylene nanoparticles. Suitable arguments for this hypothesis can be found in the literature. Here, the earlier studies of Zimmermann et al.[35,36] showed, that non-polar polymer surfaces of fluoropolymers are highly negatively charged in the presence of water. They found that hydroxide ions adsorb to the polymer surface at the interface between the solid polymer and the liquid water. Greben et al. reported on ζ potentials of polypropylene foils below −60 mV at pH 6.8.[37] In a far more general form, Creux et al. showed a strong specific hydroxide ion binding and hence negative zeta potentials at oil/water and air/water interfaces.[31] This means that negative ζ potentials can generally be expected for non-polar/water interfaces. Similarly, Nauruzbayeva et al. deduced that common hydrophobic materials such as polypropylene possess surface-bound negative charges.[38] The discussion about the existence and stability of gas-filled nanobubbles is also related.[39] Tan et al. provide a theory on how nanobubbles might survive in bulk water by a mechanism of accumulated negative surface charge density and they calculated a preferred diameter of about 200 nm.[40] Although the interpretation that the negative ζ potentials result from negative surface charges produced by adsorbed hydroxide ions is widely accepted, it should be noted here that Manning, for example, looked at this critically.[41] Uematsu et al. found in a theoretical study that the adsorption of small inorganic ions, including

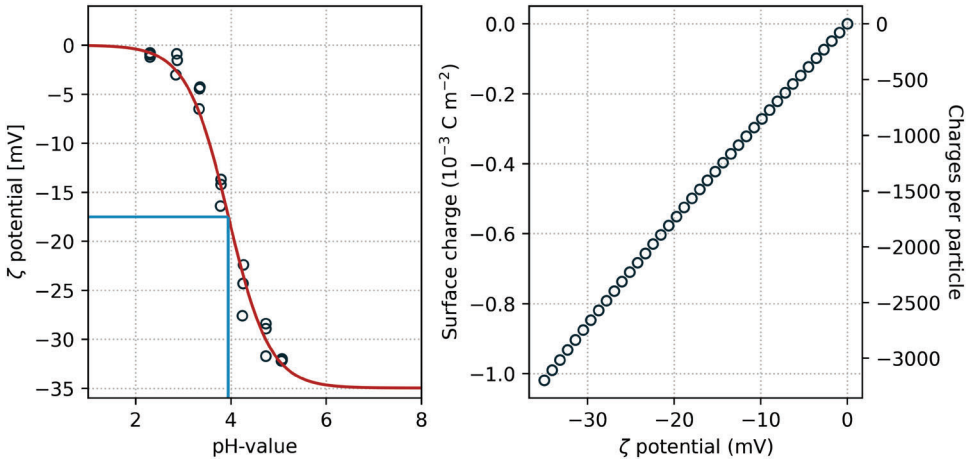

Figure 5. Left: ζ potential as a function of the pH and a curve fit according to Equation (12) (black circles and red line, respectively). The half titration pH is at pH 3.94 for which the ζ potential is 17.5 mV (indicated by blue lines). Right: Surface charge density and the number of charges (OH^- ions) per nano polypropylene particle.

hydroxide ions, cannot account for the experimentally observed negative ζ potentials of hydrophobic surfaces, although surface-active charged impurities can.[42] Even if the discussion is not yet finished, for the purpose of the present work, we adopted the common opinion and assumed that adsorbed hydroxide ions are the cause of the negative ζ potential of the nano polypropylene. Worthy of mention is the fact that we do not find a crossover from a negative to a positive surface charge for the nano polypropylene at lower pH. This contrasts with a polypropylene foil, where an isoelectric point was found around pH 4 and the zeta potential becomes positive at lower pH.[37] It can be assumed that the reason for this discrepancy is the curvature of the particle surface. Tan et al. provide an expression for the calculation of the surface charge density of bulk nanobubbles,[40] and we applied that equation to our nano polypropylene. The surface charge density of a hydrophobic particle calculates as

$$\sigma(R) = \frac{2\epsilon\epsilon_0\kappa k_B T}{e} \sinh\left(\frac{e\zeta}{2k_B T}\right) f(R) \tag{13}$$

where $\epsilon_0 = 8.854 \times 10^{-12}$ F m^{-1} is the vacuum permittivity, $\epsilon = 78.2$ is the permittivity of water at 25 °C, $e = 1.602 \times 10^{-19}$ C is the elementary charge, $k_B = 1.380649 \times 10^{-23}$ J K^{-1} is the Boltzmann constant, $T = 298$ K is the temperature (25 °C), κ is the Debye screening wave vector, and $f(R)$ is a term that corrects for the curvature of the particles. The reciprocal of κ is the Debye screening length,

$$\kappa^{-1} = \sqrt{\epsilon\epsilon_0 k_B T / 2c_0 e^2} \tag{14}$$

where c_0 is the ionic strength of the solution. For our particle dispersions with $c_0 = 1.1 \times 10^{-4}$ mol L^{-1} the Debye length is about 29 nm. Note that the theoretically possible limit (that of pure water with an ionic strength of 2×10^{-7}mol L^{-1}) is 678 nm. The $f(R)$ is a geometric term arising from an approximate solution to the spherical Poisson–Boltzmann equation,[43] given as

$$f(R) = \sqrt{1 + \frac{1}{\kappa R}\frac{2}{\cosh^2(\Psi/2)} + \frac{1}{(\kappa R)^2}\frac{8\ln\left[\cosh(\Psi/2)\right]}{\sinh^2(\Psi)}} \tag{15}$$

with the particles' radius R and

$$\Psi = e\zeta / 2k_B T. \tag{16}$$

In the large particle limit $\kappa R \gg 1$, $f(R) \to 1$ and the Equation (13) becomes the Grahame equation for a planar double layer. Application of Equation (13) provides an estimate of the surface charge density as a function of the pH value shown in the right panel of Figure 5. The surface charge density is about -1.0×10^{-3} C m^{-2} at a ζ potential of −35.0 mV (pH 7.4). This translates to an area of 156 nm^2 per OH^- ion and about 2900 OH^- ions on the surface of each particle if we assume for simplicity a spherical shape with a radius of 190 nm. The surface charge density decreases with lower ζ potential and at the half point of titration (pH 3.94) with a ζ potential of −17.5 mV the surface charge is reduced to -0.49×10^{-3} C m^{-2}.

Beattie et al.[44] estimated surface charges of -5×10^{-2} to -7×10^{-2} C m^{-2} for emulsions of hecadecane, perfluoromethyldecalin, or squalene formed at pH 7–9. These values correspond to about one hydroxide every 3 nm^2. Karraker and Radke[45] reported on one hydroxide for every 65 nm^2. Manciu and Ruckenstein[46] calculated an even lower value of about one OH^- every 167 nm^2 for an ionic strength of about 10^{-3} mol L^{-1}. The latter complies with our findings. For comparison, polymer particles which are colloidally stabilized with carboxyl or amine surface groups display much higher surface charge densities (in the order of 0.02 to 0.1 C m^{-2}) as should be expected, and as has been theoretically described by Ong et al.[47] Considering the widely diverging values in the literature, the values found here for the surface charge density seem at least plausible. We conclude from the results of the ζ potential measurements that the surface of the particles is

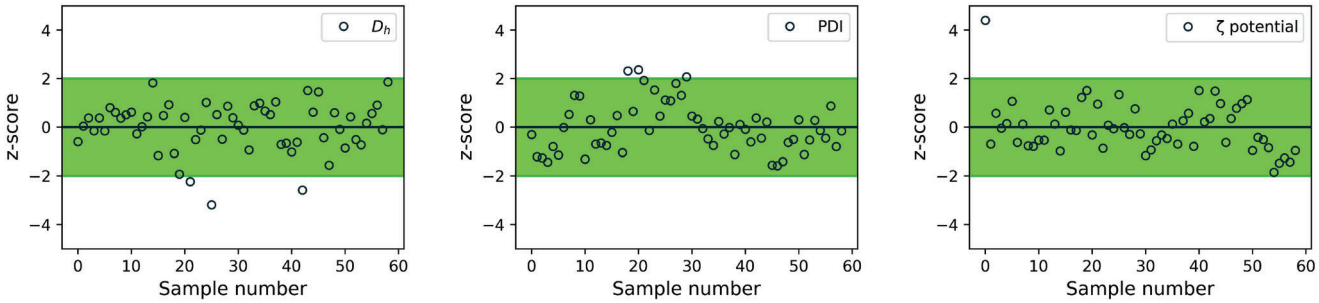

Figure 6. Repeatability of preparation of polypropylene nanoparticles. Values of *z*-scores are given for D_h, PDI, and ζ potential for all batches produced (circles). Data with *z*-scores between −2 and +2 (green area) are considered to be satisfactory. These samples were pooled to form a masterbatch.

very likely covered with hydroxyl ions, even without being able to present direct spectroscopic evidence for this. The preliminary investigations described above indicate that D_h, PDI, and ζ potential may serve as suitable quantities for nano polypropylene as reference material. The following chapters will explore this assumption further. It should be noted that all results in the following are from DLS data measured in back scattering mode at a fixed scattering angle of $2\theta = 173°$.

2.3. Repeatability

In nanotechnology, many processes fail due to their poor repeatability,[48] which could also be a problem here. Therefore, we performed a repeatability study to test our particle preparation process. For this purpose, the production of nano polypropylene was repeated 59 times to obtain statistically significant information about the repeatability of the production method. The D_h, PDI, and ζ potential were determined for a sample from each of the batches (data are provided in Supporting Information). We then compared the results of the different batches on the basis of their *z*-scores. In this study *z*-scores are calculated as

$$z = \frac{x - \bar{x}}{\sigma} \tag{17}$$

with x being the result of a measurand (D_h, PDI, and ζ potential, respectively) determined for each batch, $\bar{x}$ being the arithmetic mean of the measurand values, and σ being the standard deviation of the mean values. We refer to Lamberty et al.[49] for application of the *z*-score in an interlaboratory comparison for the measurement of the particle size and ζ potential of silica nanoparticles in an aqueous suspension. Often, *z*-scores which range within −2 and +2 are considered to be satisfactory, scores in the ± interval between 2 and 3 to be questionable, and those outside −3 and +3 to be unsatisfactory. We adopt this classification here and an overview of the resulting *z*-scores is given in **Figure 6** (circles). It can be seen that most of the values lie within the interval of −2 to 2 (satisfactory, green area) and that overall, the *z*-values of 52 of the 59 batches are within this interval for all measurands. More precisely, a number of 3 batches for D_h, 3 for PDI and 1 for ζ potential lie outside this interval and were therefore discarded. For the selected samples, the mean values are $<D_h> = 183 \pm 7$ nm, <PDI> $= 0.09 \pm 0.03$, and $<\zeta>$ potential $= -44 \pm 3$ mV. The 52 accepted batches from this repeatability study were combined into a master batch and of these a total of 480 samples were filled into glass vials (see Figure 1). The latter were taken for the assessment of homogeneity and stability.

2.4. Homogeneity

Twenty vials were randomly taken from the 480 produced vials for a homogeneity study. Samples were taken from the selected vials on three consecutive days and immediately measured, resulting in 60 values for each of the measurands D_h, PDI, and ζ potential. The overall means now are $<D_h> = 181 \pm 6$ nm, <PDI> $= 0.084 \pm 0.023$, and $<\zeta>$ potential $= -43 \pm 2$ mV. A violin plot for comparison of the measurand values for the produced batches (a), selected batches (b), and the pooled batches in the homogeneity study (c) is given in **Figure 7**. It can be seen that the mean measurand values in a, b, and c are very similar. For example, the differences of the mean values between b and c are $<D_{h,c}> - <D_{h,b}> = 2$ nm, $<PDI_c> - <PDI_b> = 0.01$ and $<\zeta_c> - <\zeta_b> = 1$ mV. These differences are smaller than the corresponding standard deviation of the means of c and b. We conclude that pooling of the selected batches to a master batch has not changed the mean values of the measurands, as was indeed expected. In contrast, from inspection of the violin plots in Figure 7 it was clear that the ranges and the standard deviations became smaller in lines a, b, and c. Therefore, the effect of selection of batches and then pooling of the selected batches is that the measurand values became more uniform, as was intended.

Of interest for the further evaluation is whether the measurand values are normally distributed. We employed Kolmogorov–Smirnov, Shapiro, and Normal tests for this purpose and found that for a and b, the hypothesis of normality for D_h, PDI, and ζ potential values could not be rejected based on these tests. Normality for D_h and ζ potential can also not be rejected for c. For PDI, however, the hypothesis of normality cannot be rejected based on the Kolmogorov–Smirnov test, but with the Shapiro and Normal tests it could be rejected. This may have been due to the narrower distribution of the values. Taken together, these tests indicate that the measurand values are normally distributed. We therefore continued the homogeneity study in the form of an analysis of variance test (ANOVA).

ANOVA was performed for the measurands according to ISO Guide 35.[50] Therein, the scattering of the values is expressed by the between-group ($M_{between}$) and within-group mean squares

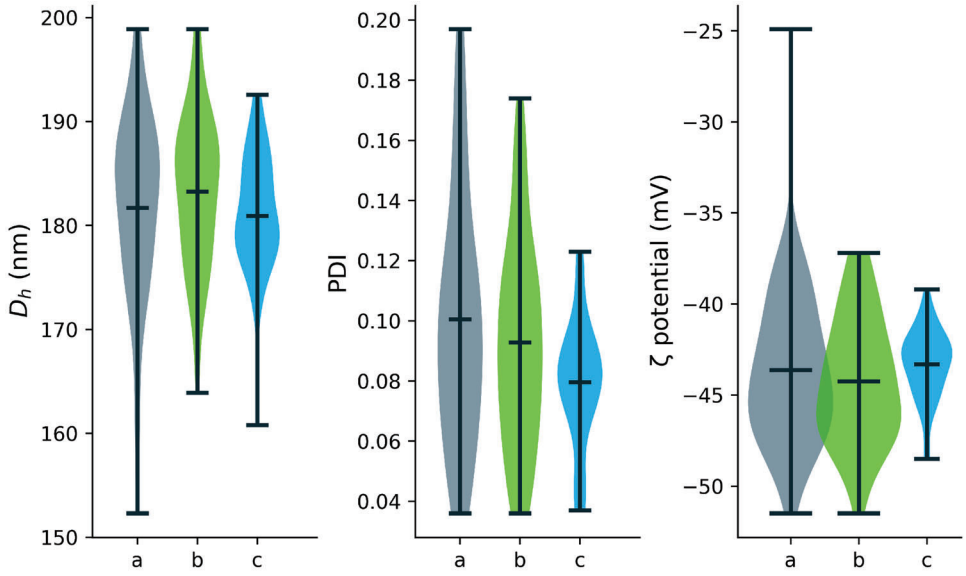

Figure 7. Violin plots of D_h, PDI, and ζ potential of nano polypropylene particles. The measurands are provided in each panel a) for all 59 batches produced, b) for the 52 selected batches, and c) for the 20 samples of the homogeneity study. Each filled area extends to represent the entire data range, with lines at the mean, the minimum, and the maximum.

Table 2. ANOVA tables for between-bottle homogeneity study of D, PDI, and ζ potential.

Overall mean (nm)	Overall s (nm)	Source of variation	SS	df	MS	s	F	F_{crit}	p-value
180.5	5.76	Between bottles	893.39	19	47.021	2.613	1.772	1.853	0.064
		Within bottles	1061.7	40	26.542	5.152			
		Total	1955.1	59					
Overall mean	Overall s	Source of variation	SS	df	MS	s	F	F_{crit}	p-value
0.084	0.023	Between bottles	0.011	19	0.001	0.004	1.102	1.853	0.385
		Within bottles	0.021	40	0.001	0.023			
		Total	0.032	59					
Overall mean (mV)	Overall s (mV)	Source of variation	SS	df	MS	s	F	F_{crit}	p-value
−42.998	1.97	Between bottles	65.07	19	3.425	0.0	0.835	1.853	0.656
		Within bottles	164.1	40	4.102	2.025			
		Total	229.17	59					

(M_{within}). These values were used for estimation of the standard uncertainties associated with between-bottle standard deviation as

$$s_{\text{bb}} = \sqrt{\max\left(\frac{M_{\text{between}} - M_{\text{within}}}{n_0},\ 0\right)} \tag{18}$$

where n_0 is the number of observations per group (here $n_0 = 3$; observation at days 1, 2, and 3). The s_{bb} is 0 if $M_{\text{between}} < M_{\text{within}}$. Furthermore, the repeatability standard deviation is calculated as

$$s_r = \sqrt{M_{\text{within}}} \tag{19}$$

The between bottle and repeatability standard deviations are $s_{\text{bb}} =$ 2.6 nm and $s_{\text{r}} = 5.1$ nm for D_{h}, $s_{\text{bb}} = 0.004$, and $s_{\text{r}} = 0.023$ for PDI and $s_{\text{bb}} = 0$ and $s_{\text{r}} = 2.0$ mV for ζ potential. Results are summarized in the ANOVA **Table 2**. An overview of the data is provided in **Figure 8**. The finding that the s_{bb} values are very small or even zero strongly indicates the absence of any between-bottle effect for D_{h}, PDI, and ζ potential. Such could be expected because all the bottles were filled from the same stock suspension. ANOVA uses a variance-based F-test to test the group mean equality. With this, the null hypothesis that all group means are equal cannot be rejected if the calculated F-value is below a tabulated critical value F_{crit}. Comparison of the data in Table 2 shows that the F-value is always $< F_{\text{crit}}$, indicating that the group means are equal. The p-values, which are inversely related to the F-values, are also given in Table 2 as indicators for significance. The p-values of 0.064 (D_{h}), 0.385 (PDI), and 0.656 (ζ potential) are larger than the typically utilized threshold value of 0.05. Therefore, the p-values are not significant, and it can be concluded that the groups have equal variances.

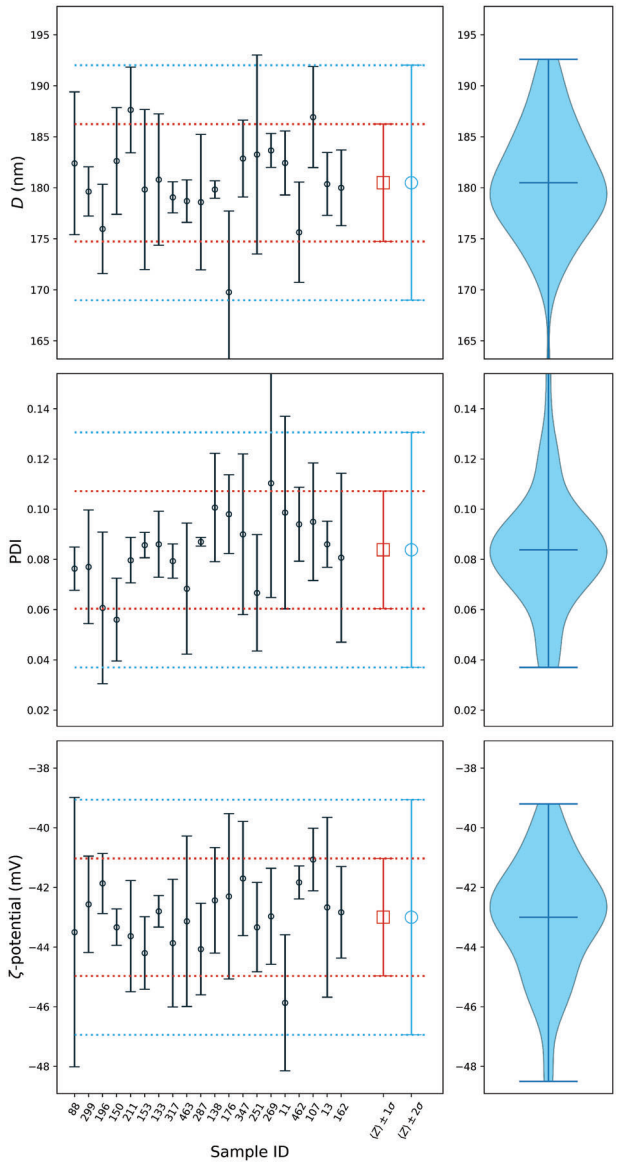

Figure 8. Homogeneity study on D_h, PDI, and ζ potential. Left panels: The 20 samples of the study are indicated by their sample IDs. Black circles and error bars represent the mean value and the standard deviation for each sample. Red squares and red error bars represent the overall mean and one standard deviation of the overall mean. Blue circles and error bars represent the overall mean and two standard deviations. Right panels: Violin plots for D, PDI, and ζ potential. Filled areas represent the entire data range.

To summarize, no evidence was observed suggesting a rejection of the hypothesis that the material is sufficiently homogeneous. In this case, the between unit homogeneity contribution to the combined uncertainty is identical to the between unit standard deviation, that is,

$$u_{bb} = s_{bb} \tag{20}$$

All data from the homogeneity study were accepted and pooled. Thus, the total mean values for the three measurands and estimates of the uncertainty u_{bb} due to possibly undetected inhomogeneity were derived from the homogeneity study. Next, the repeatability standard deviations were utilized to estimate of the uncertainty of the repeatability of a single measurement, that is,

$$u_{rep} = s_r \tag{21}$$

2.5. Stability

It might be assumed that the colloidal properties of nano polypropylene are temperature sensitive. For this reason, the candidate material was submitted for an isochronous accelerated stability study, that is, samples were measured after pre-defined storage times within short time intervals.[51] From a total of 24, 6 units each were stored at temperatures of 4, 20, 40, and 70 °C. Half of the samples were measured after a storage time of 31 days, with the rest being measured after 90 days. Inspection of the data shown in **Figure 9** suggests that D_h decreases with time, while PDI and ζ potential increase. From a colloid chemistry point of view, an increase of the ζ potential toward lower surface charge might be reasonable, because it is assumed that hydroxyl ions are responsible for the highly negative ζ potential. If the amount of OH^- ions on the surface decreases, the ζ potential increases. Also, it is typical that the PDI (size distribution width) of nanoparticles increases with storage time. What is very unusual, however, is that the hydrodynamic diameter may have reduced, since polypropylene is actually insoluble in water. Instead, increase in D_h may have been the more likely outcome, for example, due to agglomeration. It was therefore necessary to determine whether these trends were statistically significant. For this purpose, we determined Pearson correlation coefficients (r values) and p values for testing non-correlation of the measurands as a function of time. The results for each measurand and storage temperature are provided in **Table 3**. Inspection of the r values reveals that the correlation between the parameters and the storage time is low. Exceptions are only two r values of 0.750 and 0.720 for the ζ potential, which may indicate some significance for correlation. Additionally, most of the p values are much larger than the typically used threshold value of $p = 0.05$. Overall, p and r values do not provide clear indications of a statistical significance for the changes of the measurand values (at a 95% confidence level). But the lack of statistical significance for correlation does not strictly prove any absence of temperature sensitivity for the measurand values. Tentatively, for the quantitative description of the time dependence of the variables we use a simple, linear approach with

$$f(t) = k_{eff}(T)\, t + f(0) \tag{22}$$

where $k_{eff}(T)$ is a temperature-dependent proportionality coefficient and $f(0)$ is the value of the respective measurand found at the start of the stability study, that is, $t = 0$. Here, the values from the homogeneity study are utilized for $f(0)$ and held constant during curve fitting. The fit results of $k_{eff}(T)$ for D_h, PDI, and ζ potential are summarized in Table 3 and the corresponding curve fits are shown in Figure 9 (black solid lines). As expected, the $k_{eff}(T)$ values reveal large uncertainties, but nevertheless provide hints that the measurand values may change with time.

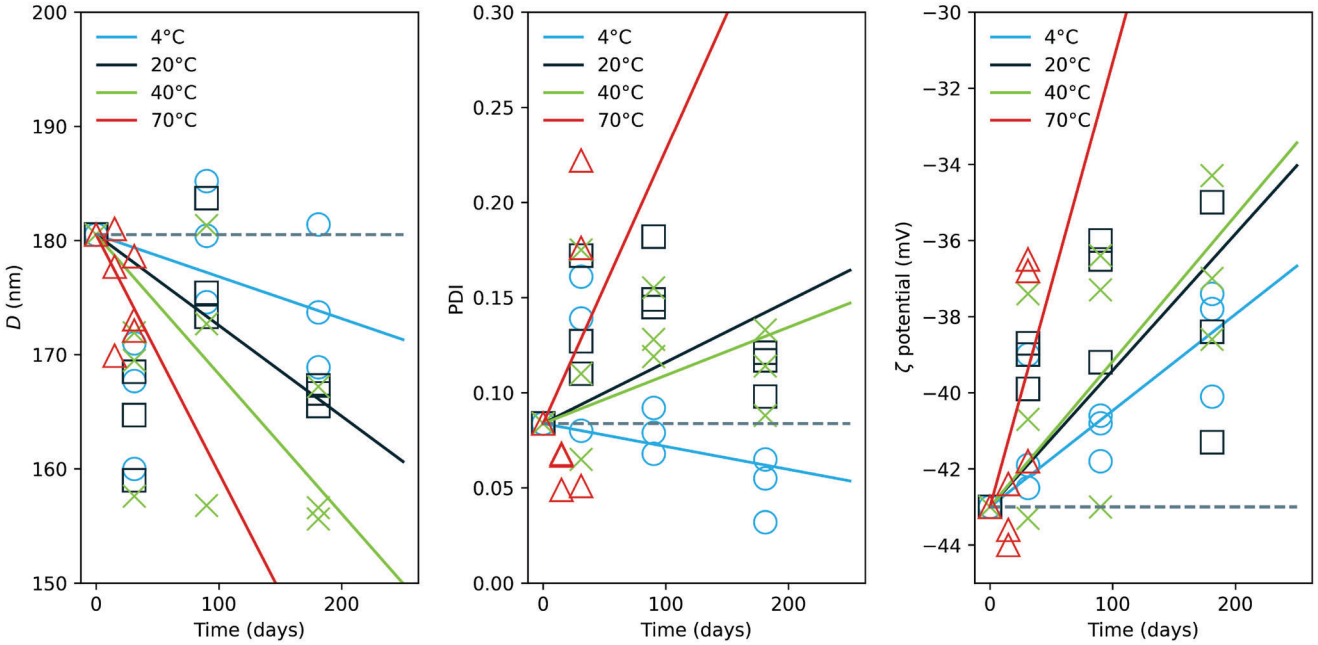

Figure 9. Accelerated stability study for D_h, PDI, and ζ potential at temperatures of 4, 20, 40, and 70 °C, measured after storage times of 0, 21, 90, and 181 days (symbols). Linear fits for estimation of k_{eff} according to Equation (22) are displayed as solid lines. Measurand values from the homogeneity study are displayed as horizontal dashed lines.

Table 3. Results of the isochronous stability study. k_{eff} is a constant describing the change of the respective parameter per month, r is the Pearson correlation coefficient, p is the p-value, $U = 2u$ is an acceptable value for the expanded uncertainty, and t_{max} is an estimate of the shelf-life.

Parameter	T [°C]	k_{eff}	r	p	U	t_{max}
D	4	−1.103 ± 0.770 nm/month	0.202	0.577	41.6 nm	38 month
D	20	−2.383 ± 0.770 nm/month	−0.180	0.618	41.6 nm	17 month
D	40	−3.663 ± 0.818 nm/month	−0.496	0.145	41.6 nm	11 month
D	70	−6.258 ± 1.997 nm/month	−0.447	0.315	41.6 nm	7 month
PDI	4	−0.004 ± 0.003 1/month	−0.696	0.026	0.2	57 month
PDI	20	0.010 ± 0.004 1/month	−0.096	0.792	0.2	21 month
PDI	40	0.008 ± 0.003 1/month	0.077	0.833	0.2	27 month
PDI	70	0.043 ± 0.031 1/month	0.526	0.225	0.2	5 month
ζ potential	4	0.759 ± 0.113 mV/month	0.750	0.013	20.4 mV	27 month
ζ potential	20	1.075 ± 0.247 mV/month	0.398	0.255	20.4 mV	19 month
ζ potential	40	1.147 ± 0.219 mV/month	0.635	0.049	20.4 mV	18 month
ζ potential	70	3.504 ± 1.219 mV/month	0.720	0.068	20.4 mV	6 month

For a reference material, it is necessary to specify an uncertainty contribution for the long-term stability u_{lts}. We therefore defined target values of u_{lts} = 20 nm (D_h), 0.1 (PDI), and 10 mV (ζ potential) as—from a practical point of view—acceptable upper limits for u_{lts}. With this, the overall uncertainty can be estimated as

$$u = \left(u_{bb}^2 + u_{rep}^2 + u_{lts}^2\right)^{1/2} \quad (23)$$

Next, the expanded uncertainty U is taken as $U = ku$ and with a coverage factor of k =2 provided U = 41.6 nm (D_h), 0.2 (PDI), and 20.4 mV (ζ potential) (see Table 3). The U and $k_{eff}(T)$ can be utilized to estimate the shelf-life

$$t_{max} = |U/k_{eff}|, \quad (24)$$

as suggested by Bremser et al.[52] This approach was applied by Riedel et al.[53] for certifying a reference material for zearalenone in maize germ oil and by Koch et al.[54] for two certified reference materials for acrylamide determination in food. Application of Equation (24) leads to estimation of the shelf-life of the nano polypropylene when stored at different temperatures. It increases from $t_{max} \approx 0.5$ to 2–3 years when decreasing the storage

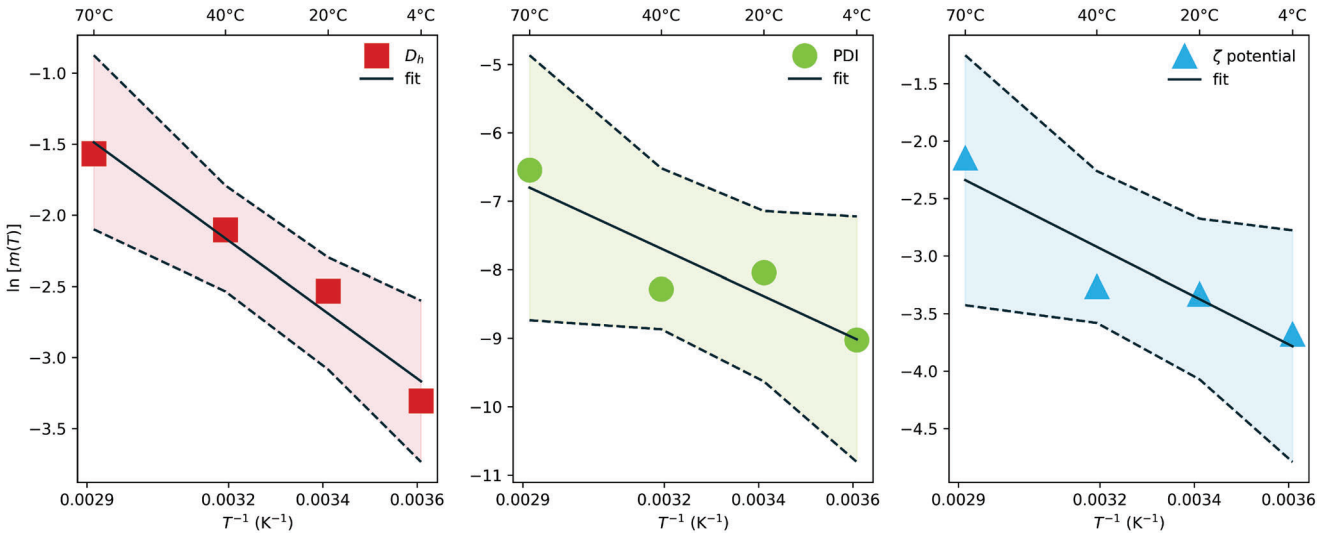

Figure 10. Arrhenius plots reveal activation energies of $E_a = -20.1 \pm 2.6$ kJ mol^{-1} for D_h, $E_a = -26.5 \pm 8.3$ kJ mol^{-1} for PDI, and $E_a = -17.3 \pm 4.7$ kJ mol^{-1} for ζ potential.

temperature from 70 to 4 °C (see Table 3). Even lower storage temperatures are utilized in the literature to increase the material's shelf-life. For example, Koch et al.[54] chose a temperature of −20 °C for storage to attain a suitable shelf-life of an acrylamide-containing reference material. Such a low storage temperature is not possible for the nano polypropylene, because the samples are not colloidally stable upon freezing. We therefore deduce that a storage temperature of 4 °C is an optimum choice for the nano polypropylene.

Although the Arrhenius model certainly represents an extensive simplification, it may serve as a rough estimate of the activation energy for the colloidal stability of nano polypropylene. Tentatively, we interpret $k_{eff}(T)$ as a temperature-dependent rate constant following an Arrhenius behavior, i.e. $k_{eff}(T) = A\exp(-E_a/(RT))$, where A is a pre-exponential factor, E_a is an activation energy of the process, and R the gas constant. Taking the natural logarithm provides

$$\ln k_{eff}(T) = \ln A - \frac{E_a}{RT} \tag{25}$$

and in a plot of $\ln k_{eff}(T)$ as a function of $1/T$ the y-intercept corresponds to $\ln A$ and the slope to $-E_a/R$. Arrhenius plots provide activation energies of $E_a = -20.1 \pm 2.6$ kJ mol^{-1} for D_h, $E_a = -26.5 \pm 8.3$ kJ mol^{-1} for PDI, and $E_a = -17.3 \pm 4.7$ kJ mol^{-1} for ζ potential (data and corresponding curve fits are shown in **Figure 10**). We are not aware of reports investigating the colloidal stability of polymer nanoparticles in terms of the Arrhenius model. However, a certain similarity may be provided by the growth of gold nanoparticles on TiO_2 and SiO_2 surfaces, for which Arrhenius plots provide activation energies of $E_a = 36 \pm 10$ kJ mol^{-1} and $E_a = 86 \pm 14$ kJ mol^{-1}, respectively.[55] Some thematically more distant examples of using Arrhenius plots for reference material development are available. An activation energy of $E_a = 53.2$ kJ mol^{-1} was reported for a certified reference material containing an estrogenic mycotoxin in maize germ oil.[53] E_a values of 47 and 60 kJ mol^{-1} were found for the degradation of acrylamide in two food reference materials.[54] The activation energies we found were somewhat lower, but at least within the same order of magnitude. A detailed understanding of the activation energy may arise from applying the recently developed fluctuation theory for dynamic systems,[56] but this is beyond the scope of the present work.

2.6. Agglomeration Profile in Salt Solution

A priori, it could have been assumed that the presence of salt reduces the colloidal stability of the suspensions because it decreases the Debye length (see Equation (14) and discussion in Section 2.2). Indeed, agglomeration was observed when the nano polypropylene was diluted with aqueous sodium chloride. Time-resolved DLS measurements were employed to monitor the agglomeration kinetics by determine the change of the hydrodynamic diameter as a function of time. We investigated suspensions with salt concentrations of c_{NaCl} =0.90% and 0.09% w/w, corresponding to molar concentrations of 150 and 15 mmol. DLS measurements were started directly after mixing the pristine particles with sodium chloride solutions in a volume ratio of 1 to 1. Examples of the resultant cumulative distribution functions (cdf) of the hydrodynamic diameters of the particles, determined after incubation times of 4, 51, and 96 min, are shown in **Figure 11** (blue, black, and green solid lines, respectively). It can be seen that the cdf shift to larger values with increasing incubation time for both salt concentrations, but the shape of the cdf differ at larger times. At times of 51 and 96 min the shape of the cdf for $c_{NaCl} = 0.90\%$ indicates a monomodal distribution while it appears bimodal for $c_{NaCl} = 0.09\%$. We interpret these shifts as resultant from the appearance of agglomerates of primary particles, which were held together by van der Waals interactions. In addition to the presence of agglomerates, a considerable number of non-agglomerated particles seem to be still present at the lower salt concentration. The monomodal and bimodal

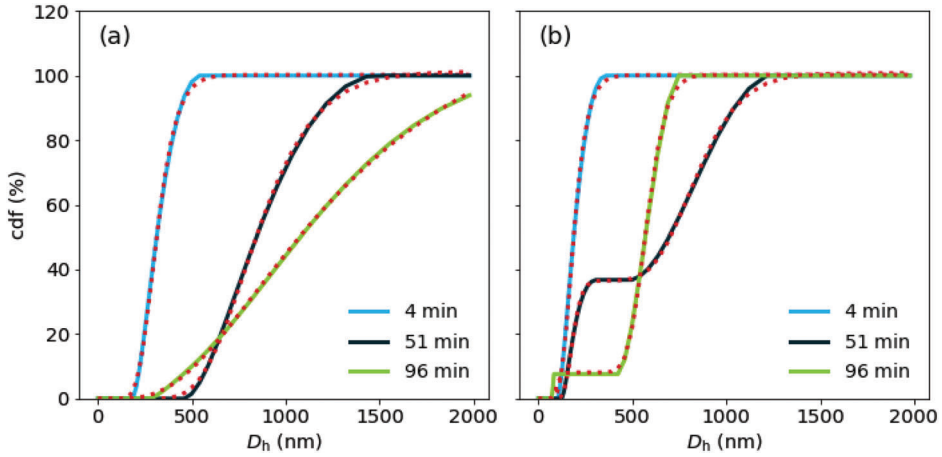

Figure 11. Time evolution of the cumulative distribution function (cdf) of the hydrodynamic diameters during storage of nano polypropylene in sodium chloride solution with concentrations of a) $c_{NaCl} = 0.90$ and b) $c_{NaCl} = 0.09$. Displayed are cdfs for incubation times of 4 min (blue), 51 min (black), and 96 min (green). Curve fits according to Equation (26) are provided as red dotted lines.

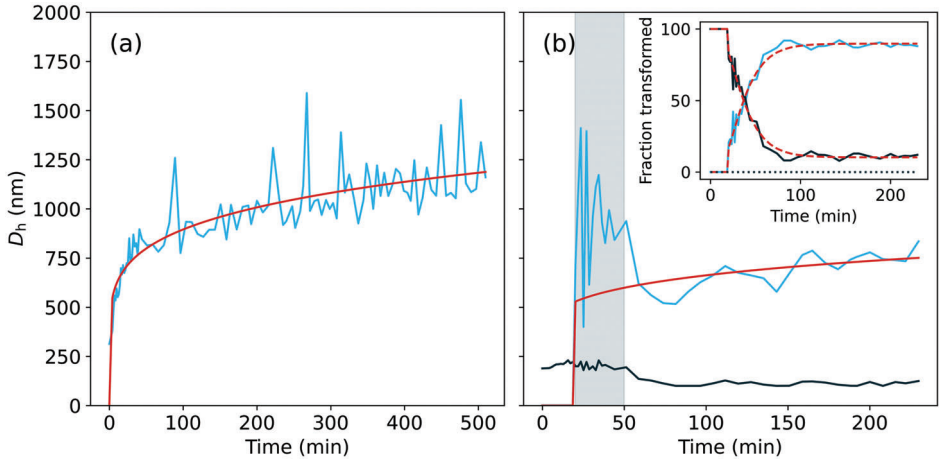

Figure 12. Time evolution of the median values of the hydrodynamic diameters of nano polypropylene at salt concentrations of a) $c_{NaCl} = 0.90$ and b) $c_{NaCl} = 0.09$. The change of the hydrodynamic diameter of the agglomerates (blue lines) were approximated using Equation (27) (red solid lines, gray are in panel (b) was not included in curve fitting). Inset: Fraction of particles transformed to agglomerates and non-agglomerated particles (blue and black solid line). Curve fits accordingly are given as red dashed lines.

distributions were described by one, respectively, by two cumulative lognormal distribution functions as

$$f(D_h) = \sum_{i=1}^{n} \frac{a_i}{n} \mathrm{erf}\left(\frac{\log\left(\frac{D_h}{D_{h,i}}\right)}{\sqrt{2} w_i} \right) \quad (26)$$

with $n = 1$ for $c_{NaCl} = 0.9\%$ and $n = 2$ for $c_{NaCl} = 0.09\%$. The a_i are scaling factors, which are a measure of the fraction of particle population i, respectively. The w_i are width parameters and the $D_{h,i}$ are the median hydrodynamic diameter. The experimental curves were fitted well by employing Equation(26) as shown exemplarily as red dashed lines in Figure 11a,b. The resultant $D_h(t)$ data are displayed in **Figure 12**a,b (blue lines for agglomerates, black line for non-aggregated particles). It can be seen that agglomerations are immediately formed and monotonically grow at the higher salt concentration. At the lower salt concentration, non-agglomerated particles are present at all incubation times (black solid line in the right-hand panel of Figure 12). Here, the agglomeration process may be divided in different temporal stages (see blue line). First, no agglomerates are found in an induction period of $t_0 = 20$ min. Then, loose but large agglomerates are formed in the period between 20 and 50 min with large size fluctuations up to about 1 micron (displayed gray). Afterward, at times of about 50 min, compaction of the agglomerates takes place to sizes of about 500 to 600 nm. Finally, for times longer than 50 min, the more compacted agglomerates grow slowly in size. For interpretation of the time evolution of the size of the agglomerates, the power law

$$D_h(t) = D_{h,0} + k_D\,(t - t_0)^{\alpha} \quad (27)$$

was employed, where $D_{h,0}$ is the initial hydrodynamic diameter of the particles of 189 nm, k_D is an effective aggregation constant, and α is the power law exponent. The parameter t_0 is the time at which the aggregation starts, that is, $t_0 = 0$ and 20 min,

respectively. Equation (27) appears reasonable for modeling $D_h(t)$ as shown in Figure 12a,b (red solid lines). The best fit curves provide k_D values of (265 ± 24) nm min^{-1} (c_{NaCL} = 0.90%) and k_D = (182 ± 65) nm min^{-1} (c_{NaCL} = 0.09%). The considerably higher value of k_D at the higher salt concentration shows that the agglomeration proceeds much faster at higher salt concentration than at lower ones. Such was expected, because a salt induced increase of agglomeration and aggregation of particles in suspensions has been reported for numerous suspensions.[57,58] In contrast to k_D, the corresponding values for the exponent α = 0.21 ± 0.02 and 0.21 ± 0.07 are the same. This indicates that the type of agglomerate formation is not affected by the salt concentration.[58] For the bimodal case (c_{NaCl} =0.09%), the scaling factors (a_1 and a_2) in Equation (26) are measures for the fraction of particles transformed to aggregates and non-aggregated particles. The course of the fraction of the transformed particles and non-aggregated particles is shown in the inset of Figure 12 (blue and black solid line, respectively). It can be seen that the agglomeration essentially takes place in the time interval of 20 to 100 min. A simulation of the increase of the fraction of transformed particles, c_{rel}, was performed by

$$c_{rel}(t) = c_\infty \left(1 - e^{-k_c(t-t_0))}\right)^n \quad (28)$$

which provides a final relative amount of particles transformed to agglomerates of c_∞ = (89 ± 1)%, the apparent transformation rate constant is k_c = (0.05 ± 0.01) min^{-1}, the delay time is t_0 = 20 min (was held constant) and the exponent is n = 4.2 ± 0.7. The curve fit for $c_{rel}(t)$ and the relative amount of non-aggregated particles (1-$c_{rel}(t)$) is shown in the inset of Figure 12 (red dashed lines).

3. Summary and Outlook

In summary, we report here on an aqueous dispersion of colloidally stable polypropylene nanoparticles. The stability is interpreted in terms of a highly negative ζ potential, likely resulting from hydroxyl ions present at the particles' surface. The particle preparation method was described in detail with respect to its repeatability, as was the study of homogeneity and stability of the dispersions. In the present study, a polypropylene with a low molar mass of M_w = 12000 g mol^{-1} was used for particle preparation. The tentative use of polypropylene with a considerably higher molar mass of M_w = 250000 g mol^{-1} lead to particles with a very similar distribution of hydrodynamic diameters (see Figure S3, Supporting Information for comparison). Therefore, it can be assumed that the particle preparation method can at least be transferred to polypropylene with other molar masses. The particles are intended to be used in further studies developing analytical methods to characterize and quantify polypropylene nanoparticles in the environment. Furthermore, the particles may also be used to study the fate of polypropylene nanoparticles in biologically relevant surroundings, for example, with their uptake by cell cultures. The particles start to agglomerate when immersed into sodium chloride solution. Agglomeration is faster at higher salt concentration. However, this is not a disadvantage for the intended use as reference material in cell cultures, as the biological effect of agglomerates is of particular interest here. The particle preparation method is also intended to be used for producing nanoplastic reference materials made of the remaining five "Big Six" polymers, that is, PE, PVC, PU, PET, and PS.

4. Experimental Section

Materials: All chemicals were used as received without further purification. Polypropylene (isotactic, average $\bar{M}_w \approx$ 12000g mol^{-1}, average $\bar{M}_n \approx$ 5000g mol^{-1} and isotactic, average $\bar{M}_w \approx$ 250000g mol^{-1}, average $\bar{M}_n \approx$ 67000g mol^{-1}) was purchased from Sigma-Aldrich. Acetone (p.A., min. 99.5 %, ChemSolute) was purchased from Th.Geyer. The water for the preparation was purified using a Sartorius arium 611DI purifier. Folded filters of grade 2105 (fast filtering, particle retention 12–15µm, by LabSolute) were purchased from Th.Geyer.

DLS Measurements: DLS measurements were performed using a multi-angle ALV 7004 device with a He-Ne laser (λ =632.8nm) from ALV Langen. The samples were filtered using a Millex 0.45µm PVDF syringe filter. The glass cuvettes used were cleaned with acetone prior to filling them with the sample. Measurements were performed at scattering angles of 2θ =26°–146° in 8° steps and at a temperature of 20 ± 1°C. Three measurements, lasting 30 s each, were carried out at each angle. The magnitude of the scattering vector is given by $q = 4\pi n/\lambda \sin\theta$ where n = 1.333 is the refractive index of water. Measurement of D_h, PDI, and ζ potential for the homogeneity and stability studies were performed with an instrument working in back scattering geometry at an angle of 2θ = 173° (Zetasizer from Malvern Panalytical). Six measurements were taken on each sample.

GPC Measurements: This analytical method describes the determination of the molar masses and molar mass distribution of polyolefins after gel chromatographic separation on GPC columns (3 × PSS POLYOLEFIN linear XL, 30 × 0.8 cm, 10 µm pore size). This method was a relative method. The molar masses were calculated based on a universal calibration with 12 polystyrene standards from Polymer Standards Service GmbH, over the range of $M_p = 1.2 \cdot 10^7 - 266$ g mol^{-1} by conversion according to Mark–Houwink parameters. A high-temperature GPC equipped with infrared (IR4) and viscosity detection (PolymerChar GPC-IR), an isocratic HPLC pump (PSS-Security), and an autosampler from PolymerChar GPC-IR running at 160°C were used. The eluent used was 1,2,4-trichlorobenzene stabilized with 0.1 % BHT. The flow rate was 1.0 mL min^{-1}. Injection of 200 µL of an approximately 2 mg mL^{-1} (8 mL total) solution in the eluent (internal filtration unit) then followed. The error range was estimated at approximately ± 10%.

SEM Experiments: SED was performed with a Zeiss Supra 40 Scanning Electron Microscope (Zeiss, Oberkochen, Germany), at 10 kV acceleration voltage, 4.8 mm WD, in SE InLens mode, and at different magnifications. Before measurement, the flask with nano polypropylene was carefully shaken. 3 µL of the suspension (PP, ID336) were drop-casted on the carbon tape and allowed to dry for ca. 24 h under normal laboratory conditions.

Zeta Potential Measurements: ζ potential measurements were performed using a ZetaSizer Nano ZS and MPT-2 titrator (both Malvern Panalytical). The sample holder was equipped with a folded capillary cell (DTS1070 cell). After a single ζ potential measurement for sample quality checking, the cell was connected via tubing to the titrator. The titrator was filled with deionized water and two solutions of hydrochloric acid (c_1 =0.25 mol L^{-1} and c_2 =0.01 mol L^{-1}) for titration to lower pH values. All solutions used for these measurements were filtered prior to use with a Millex 0.45 µm PVDF syringe filter. A temperature of 25 °C was maintained during the measurements. For every pH step, 3 measurements were performed. The titration was started at the initial pH of the sample and carried out down to a pH of 2. The titration steps were approximately pH = 0.5. For measurements related to the repeatability and homogeneity tests, the ζ potential was measured according to the single measurement automatic procedure.

Top-Down Preparation of Nanoplastics: The polypropylene granules (6.0 g) were added to a glass beaker (tall-form) before acetone (115 mL) was added (diameter of the granules was ca. 5 mm). The beaker was cooled with an ice bath to prevent the evaporation of acetone during the

preparation. The polymer granules were dispersed with a disperser (IKA T 18 digital ULTRA-TURRAX) for 10 min at a rotation speed of 18000 rpm. After dispersion, the solution was filtered using a folded filter to remove the larger aggregates of the polymer. Acetone was evaporated until ca. 10 % of the liquid remained. Then water (115 mL) was added to the mixture and the remaining acetone was evaporated to obtain an aqueous dispersion of the polymer nanoparticles. The aqueous dispersion was again filtered with a folded filter, to remove any particles that may have aggregated while being transferred to the water. An overview on the particle preparation is provided in Figure S1, Supporting Information.

Preparation of the Reference Material: The reference material was prepared according to the method described above. The preparation was repeated several times and all batches with a z-score between −2 and +2 (see Figure 6) were added to a 5 L bottle. The stock bottle was swirled to mix the batches. The bottle was equipped with a BRAND seripettor bottletop dispenser with a dispensing volume of 10 mL. The reference material was dispensed into small screw-top glass bottles. After every 15th filling, the stock bottle was swirled again to maintain a good mixture. Finally, 481 bottles with a sample volume of 10 mL each were filled with the reference material (see Figure 1). To improve durability, the samples were pasteurized in an oven at 90 °C for 2 h. These samples were then used for the homogeneity tests.

Gravimetric Analysis of the Polymer Concentration: An aluminum open sample pan (for DSC measurements) was weighed empty. It was heated to 150 °C on a hot plate. After this, a 1 mL aliquot of the sample was added dropwise to the sample pan while the pan was still heated. Care was taken to ensure that no drop landed outside the sample pan. Finally, the sample pan was heated for another 15 min to remove any possible residual liquid. The sample pan was weighed again and the difference determined. Gravimetric concentration determination was performed three times. The concentration of polymer in the dispersion was 41 ± 4 mg L^{-1}.

Supporting Information

Supporting Information is available from the Wiley Online Library or from the author.

Acknowledgements

The authors thank Malte Wulff for helping with the adaption of the preparation method and Tina Rybak, Maximilian Ebisch, and Kai Simon Rother for the preparation of the nanoplastic samples. In addition, the authors thank Ralf Bienert for assistance with the ζ potential measurements, Jana Falkenhagen and Karin Böttcher for performing the AF4 and GPC measurements, and Vasile-Dan Hodoroaba and Dmitri Ciornii for carrying out the SEM measurements.

Open Access funding enabled and organized by Projekt DEAL.

Conflict of Interest

The authors declare no conflict of interest.

Data Availability Statement

The data that support the findings of this study are available from the corresponding author upon reasonable request.

Keywords

nanoplastics, polypropylene, reference materials

Received: November 8, 2022
Revised: December 1, 2022
Published online: January 5, 2023

[1] S. Wagner, T. Reemtsma, *Nat. Nanotechnol.* **2019**, *14*, 300.
[2] R. Geyer, J. R. Jambeck, K. L. Law, *Sci. Adv.* **2017**, *3*, e1700782.
[3] N. B. Hartmann, T. Huffer, R. C. Thompson, M. Hassellov, A. Verschoor, A. E. Daugaard, S. Rist, T. Karlsson, N. Brennholt, M. Cole, M. P. Herrling, M. C. Hess, N. P. Ivleva, A. L. Lusher, M. Wagner, *Environ. Sci. Technol.* **2019**, *53*, 1039.
[4] M. B. Paul, C. Fahrenson, L. Givelet, T. Herrmann, K. Loeschner, L. Böhmert, A. F. Thünemann, A. Braeuning, H. Sieg, *Microplastics Nanoplastics* **2022**, *2*, 16.
[5] A. A. Koelmans, E. Besseling, W. J. Shim, *Nanoplastics in the Aquatic Environment. Critical Review, Marine Anthropogenic Litter*, Springer, Cham **2015**.
[6] I. Paul-Pont, K. Tallec, C. Gonzalez-Fernandez, C. Lambert, D. Vincent, D. Mazurais, J.-L. Zambonino-Infante, G. Brotons, F. Lagarde, C. Fabioux, P. Soudant, A. Huvet, *Front. Mar. Sci.* **2018**, *5*, 252.
[7] L. Frère, I. Paul-Pont, E. Rinnert, S. Petton, J. Jaffré, I. Bihannic, P. Soudant, C. Lambert, A. Huvet, *Environ. Pollut.* **2017**, *225*, 211.
[8] J. Gigault, A. T. Halle, M. Baudrimont, P.-Y. Pascal, F. Gauffre, T.-L. Phi, H. El Hadri, B. Grassl, S. Reynaud, *Environ. Pollut.* **2018**, *235*, 1030.
[9] K. Tallec, A. Huvet, C. Di Poi, C. González-Fernández, C. Lambert, B. Petton, N. Le Goïc, M. Berchel, P. Soudant, I. Paul-Pont, *Environ. Pollut.* **2018**, *242*, 1226.
[10] O. Hollóczki, S. Gehrke, *ChemPhysChem* **2020**, *21*, 9.
[11] O. Hollóczki, S. Gehrke, *Sci. Rep.* **2019**, *9*, 16013.
[12] L. Pessoni, C. Veclin, H. El Hadri, C. Cugnet, M. Davranche, A.-C. Pierson-Wickmann, J. Gigault, B. Grassl, S. Reynaud, *Environ. Sci. Nano* **2019**, *6*, 2253y.
[13] O. Pikuda, E. G. Xu, D. Berk, N. Tufenkji, *Environ. Sci. Technol. Lett.* **2019**, *6*, 21.
[14] S. Reynaud, A. Aynard, B. Grassl, J. Gigault, *Curr. Opin. Colloid Interface Sci.* **2022**, *57*, 101528.
[15] M. T. Ekvall, M. Lundqvist, E. Kelpsiene, E. Šileikis, S. B. Gunnarsson, T. Cedervall, *Nanoscale Adv.* **2019**, *1*, 1055.
[16] M. T. Ekvall, I. Gimskog, J. Hua, E. Kelpsiene, M. Lundqvist, T. Cedervall, *Sci. Rep.* **2022**, *12*, 3109.
[17] S. Bhattacharjee, *J. Controlled Release* **2016**, *235*, 337.
[18] F. Lionetto, C. Esposito Corcione, A. Rizzo, A. Maffezzoli, *Polymers* **2021**, *13*, 21.
[19] W. M. Haynes, *CRC Handbook of Chemistry and Physics*, Vol. *97*, CRC Press, Boca Raton, FL **2016**.
[20] A. Guinier, G. Fournet, *Small-Angle Scattering of X-Rays*, John Wiley & Sons, Inc., New York **1955**.
[21] B. J. Frisken, *Appl. Opt.* **2001**, *40*, 4087.
[22] D. E. Koppel, *J. Chem. Phys.* **1972**, *57*, 4814.
[23] W. Brown, *Dynamic Light Scattering - The Method and Some Applications*, Clarendon Press, Oxford **1993**.
[24] Standardization fIO. ISO 22412:2017(E) Particle size analysis - Dynamic light scattering (DLS),*ISO* **2017**.
[25] BIPM. Evaluation of measurement data - Guide to the expression of uncertainty in measurement (GUM), JCGM 100 **2008**.
[26] W. Schärtl, *Light Scattering from Polymer Solutions and Nanoparticle Dispersions*, Springer Laboratory Manuals in Polymer Science, Springer Berlin, Heidelberg **2007**.
[27] J. Stetefeld, S. A. McKenna, T. R. Patel, *Biophys. Rev.* **2016**, *8*, 409.
[28] J. G. Delatorre, S. Navarro, M. C. L. Martinez, *Biophys. J.* **1994**, *66*, 1573.
[29] R. Pecora, *J. Nanopart. Res.* **2000**, *2*, 123.
[30] C. Jacobs, R. H. Muller, *Pharm. Res.* **2002**, *19*, 189.
[31] P. Creux, J. Lachaise, A. Graciaa, J. K. Beattie, A. M. Djerdjev, *J. Phys. Chem. B* **2009**, *113*, 14146.
[32] V. Patel, Y. Agrawal, *J. Adv. Pharm. Technol. Res.* **2011**, *2*, 81.
[33] W. Brown, J. X. Zhao, *Macromolecules* **1993**, *26*, 2711.
[34] U. Dippon, S. Pabst, S. Klitzke, *Sci. Total Environ.* **2018**, *645*, 1153.

[35] R. Zimmermann, N. Rein, C. Werner, *Phys. Chem. Chem. Phys.* **2009**, *11*, 4360.
[36] R. Zimmermann, U. Freudenberg, R. Schweiß, D. Küttner, C. Werner, *Curr. Opin. Colloid Interface Sci.* **2010**, *15*, 196.
[37] K. Greben, P. G. Li, D. Mayer, A. Offenhausser, R. Wordenweber, *J. Phys. Chem. B* **2015**, *119*, 5988.
[38] J. Nauruzbayeva, Z. H. Sun, A. Gallo, M. Ibrahim, J. C. Santamarina, H. Mishra, *Nat. Commun.* **2020**, *11*, 5285.
[39] N. Nirmalkar, A. W. Pacek, M. Barigou, *Langmuir* **2018**, *34*, 10964.
[40] B. H. Tan, H. J. An, C. D. Ohl, *Phys. Rev. Lett.* **2020**, *124*, 13.
[41] G. S. Manning, *Phys. Chem. Chem. Phys.* **2020**, *22*, 17523.
[42] Y. Uematsu, D. J. Bonthuis, R. R. Netz, *Langmuir* **2020**, *36*, 3645.
[43] K. Makino, H. Ohshima, *Langmuir* **2010**, *26*, 18016.
[44] J. K. Beattie, A. N. Djerdjev, G. G. Warr, *Faraday Discuss.* **2009**, *141*, 31.
[45] K. A. Karraker, C. J. Radke, *Adv. Colloid Interface Sci.* **2002**, *96*, 231.
[46] M. Manciu, E. Ruckenstein, *Adv. Colloid Interface Sci.* **2003**, *105*, 63.
[47] G. M. C. Ong, A. Gallegos, J. Wu, *Langmuir* **2020**, *36*, 11918.
[48] R. E. Abutbul, Y. Golan, *Nanotechnology* **2021**, *32*, 10.
[49] A. Lamberty, K. Franks, A. Braun, V. Kestens, G. Roebben, T. P. J. Linsinger, *J. Nanopart. Res.* **2011**, *13*, 7317.
[50] ISO GUIDE 35, ISO GUIDE 35:2017(E) Reference materials - Guidance for characterization and assessment of homogeneity and stability, *ISO* **2017**, 105.
[51] J. Pauwels, A. Lamberty, H. Schimmel, *Fresenius J. Anal. Chem.* **1998**, *361*, 395.
[52] W. Bremser, R. Becker, H. Kipphardt, P. Lehnik-Habrink, U. Panne, A. Töpfer, *Accredit. Qual. Assur.* **2006**, *11*, 489.
[53] J. Riedel, S. Recknagel, D. Sassenroth, T. Mauch, S. Buttler, T. Sommerfeld, S. Penk, M. Koch, *Anal. Bioanal. Chem.* **2021**, *413*, 5483.
[54] M. Koch, W. Bremser, R. Koeppen, D. Siegel, A. Toepfer, I. Nehls, *J. Agric. Food Chem.* **2009**, *57*, 8202.
[55] N. Masoud, T. Partsch, K. P. de Jong, P. E. de Jongh, *Gold Bull.* **2019**, *52*, 105.
[56] Z. A. Piskulich, O. O. Mesele, W. H. Thompson, *J. Phys. Chem. A* **2019**, *123*, 7185.
[57] L. T. T. Trinh, A. L. Kjoniksen, K. Z. Zhu, K. D. Knudsen, S. Volden, W. R. Glomm, B. Nystrom, *Colloid Polym. Sci.* **2009**, *287*, 1391.
[58] R. Pamies, J. G. H. Cifre, V. F. Espin, M. Collado-Gonzalez, F. G. D. Banos, J. G. de la Torre, *J. Nanopart. Res.* **2014**, *16*, 2376.

Macromolecular Rapid Communications

Supporting Information

for *Macromol. Rapid Commun.*, DOI 10.1002/marc.202200874

Aqueous Dispersions of Polypropylene: Toward Reference Materials for Characterizing Nanoplastics

*Jana Hildebrandt and Andreas F. Thünemann**

Aqueous Dispersions of Polypropylene: Towards Reference Materials for Characterizing Nanoplastics

*Jana Hildebrandt, Andreas F. Thünemann**

SUPPORTING INFORMATION

FIGURE 1 Photographs taken of the steps of the nano polypropylene preparation. a) Dispersing the PP in acetone with a Ultra-Turrax disperser (18000 rotations min^{-1} for 10 min). The acetone is cooled with ice (0°C) to keep the acetone from evaporating. b) After dispersion, the disperser tool is cleaned with 5 ml acetone. c) Micro and macroscopic residue is separated with a folded filter (pore size of 12 to 15 micrometer). d) An amount of 90 % of the acetone was evaporated; the remaining 15 ml of dispersion in acetone is indicated with the blue circle. e) The addition of 115 ml of water leads to an immediate turbidity of the dispersion. f) After removing the remaining acetone, the dispersion was filtered again to remove possible aggregation products.

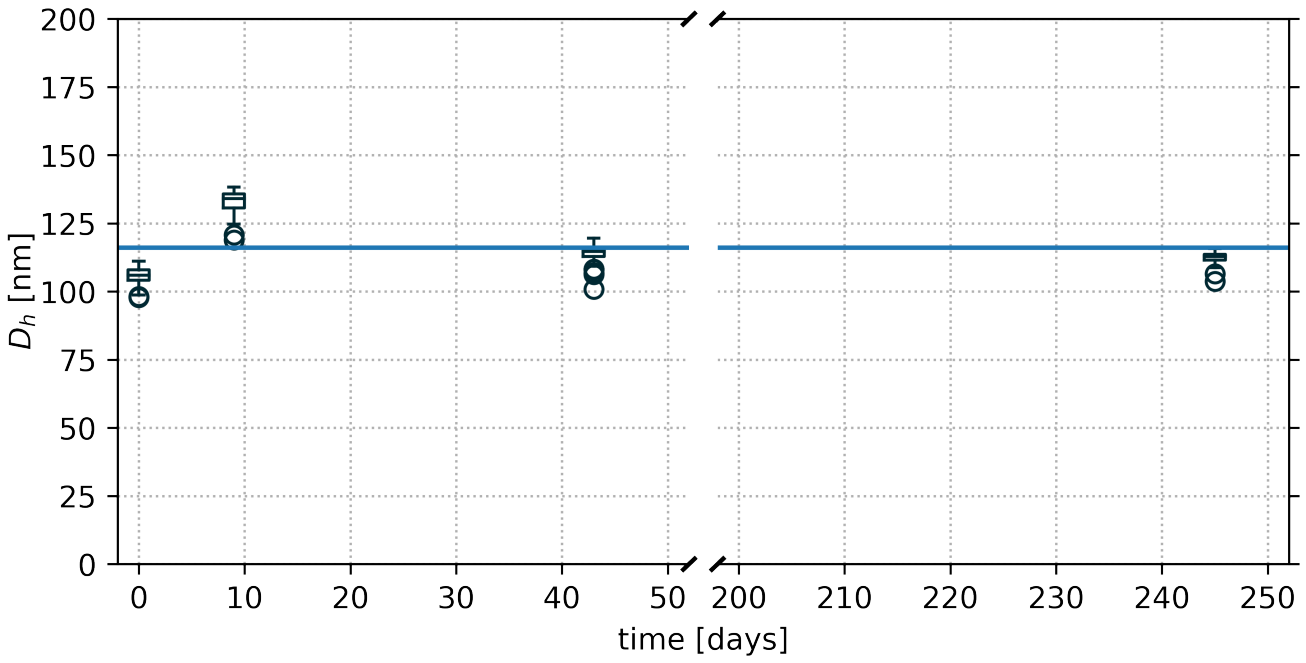

FIGURE 2 Hydrodynamic diameter of a preliminary test sample at storage times of 0, 9, 43 and 245 days after preparation of the sample. The mean value of the hydrodynamic diameter of this sample is 116 ± 10 nm (horizontal line).

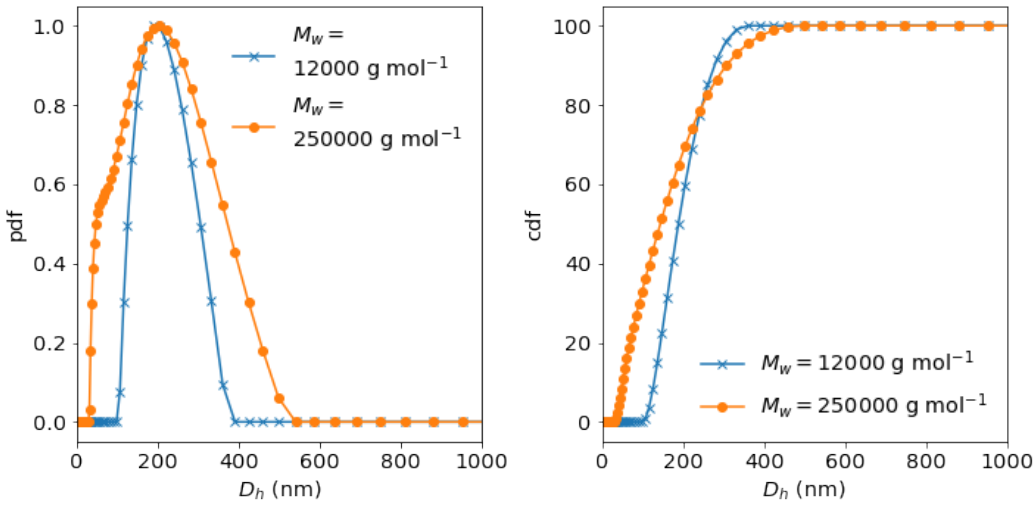

FIGURE 3 Intensity weighted distributions of the hydrodynamic diameter of nano polypropylene, displayed as probability distribution functions (pdf) and cumulative distribution functions (cdf). The particles were prepared from polypropylene with molar mass characteristics of M_w = 12000 g mol^{-1} and M_n = 7000 g mol^{-1} (yellow circles) and a molar mass characteristics of M_w = 250000 g mol^{-1} and M_n = 67000 g mol^{-1} (blue crosses).

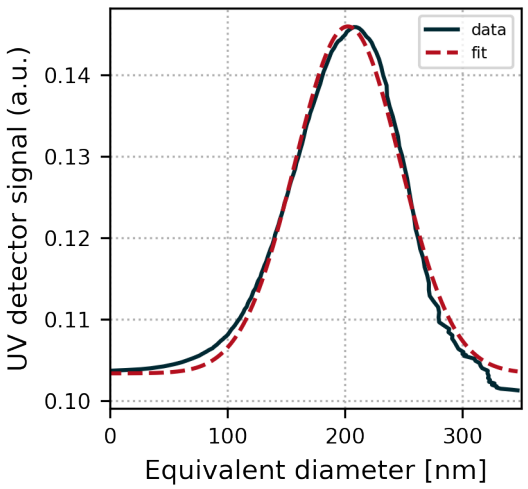

FIGURE 4 A4F results: Distribution of the equivalent diameters of nano polypropylene particles (black, solid line) and curve fit with a Gaussian distribution (red, dashed line) with a maximum at 202 ± 1 nm and a width of 44 ± 1 nm.